Numerical issues on brittle shear failure of pier-wall continuous vertical joints in URM dutch buildings

Fusco, Daniela; Messali, Francesco; Rots, Jan G.; Addessi, Daniela; Pampanin, Stefano

DOI
10.1016/j.engstruct.2022.114078

Publication date
2022

Document Version
Final published version

Published in
Engineering Structures

Engineering Structures 258 (2022) 114078

Contents lists available at ScienceDirect

Engineering Structures

journal homepage: www.elsevier.com/locate/engstruct

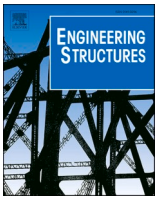

Numerical issues on brittle shear failure of pier-wall continuous vertical joints in URM dutch buildings

Daniela Fusco [a,*], Francesco Messali [b], Jan G. Rots [b], Daniela Addessi [a], Stefano Pampanin [a]

[a] Sapienza Università di Roma, Dipartimento di Ingegneria Strutturale e Geotecnica Via Eudossiana 18, 00184 Rome, Italy
[b] Delft University of Technology, Department 3MD, Building 23, Stevinweg 1, 2628 CN Delft, the Netherlands

ARTICLE INFO

Keywords:
Unreinforced masonry
Continuous vertical joints
Numerical modelling
Constitutive models

ABSTRACT

Terraced houses built in the Netherland after 1980 are often characterized by the use of large units connected at corners by continuous thin layer mortar joints. Unlike the running bond pattern, usually modelled as a rigid connection, the vertical continuous connection may fail in shear and influence the global seismic capacity of the entire building. This work aims at investigating and comparing different numerical modelling approaches for simulating the vertical connections. Two different constitutive models are adopted to simulate the quasi-brittle nonlinear behaviour of the continuous joint, and their advantages and limitations are pointed out in terms of robustness and accuracy. The study considers both the component level in terms of U-shaped pier-wall configuration, and the full-scale structural level in terms of the global capacity for a two-storey masonry house assemblage, characterized by a running bond arrangement. The results of this work show that the shear failure involving the continuous joint usually reduces the strength capacity of the structure. Both the selection of constitutive models for the connection interface and masonry material are demonstrated to affect the results significantly. Decoupled direct traction-displacement relations for the interfaces appear to provide more robust results than coupled plasticity-based Coulomb friction laws. The selection of either a pre-fixed orthotropic smeared crack model for the masonry or a standard isotropic concrete-like rotating smeared crack formulation is demonstrated to strongly influence the activation of the different failure mechanisms and hence the response of the structure.

1. Introduction

The unreinforced masonry (URM) terraced houses represent a large part of the building stock in the north of the Netherlands. These buildings are characterized by slender piers and large openings on the façades, and long walls in the transversal direction. Unlike many other URM structures, in several terraced houses built around the 1960s the spandrels and the window banks do not have a structural function, being disconnected from the piers, so that the seismic resisting structure is represented only by the piers on the façades and the transversal walls.

The Dutch terraced houses built after the 1960s are characterized by the use of calcium silicate (CS) masonry, and piers and transversal walls can be assumed strongly connected due to the use of the running bond pattern. Since the 1980s, the traditional small CS bricks were replaced by large CS elements, and the connections between walls and piers consisted of vertical continuous thin layer mortar joints. Usually cement-based mortar with high compressive resistance and limited thickness (2–3 mm) is used, and often flat steel ties are embedded at the bed-joint level, as illustrated in Fig. 1. These ties are able to provide an efficient tensile restraint, but they do not have any significant shear stiffness due to the limited thickness and are not able to prevent or postpone significantly the shear failure along the joint.

In common practice, the pier-wall connections at the corners of masonry buildings are modelled as rigid. This assumption may be valid in case of a running bond pattern, but it may lead to an overestimation of the capacity of the building in case of continuous vertical joints. In fact, the failure of these latter considerably decreases the seismic capacity of the URM structure [1].

An experimental campaign conducted by Raijmakers and Van der Pluijm [2] investigated the possible failures of a U-shaped subassemblage, composed by two slender piers connected to the transversal wall through a continuous vertical connection. This experimental

* Corresponding author.
E-mail addresses: daniela.fusco@uniroma1.it (D. Fusco), F.Messali@tudelft.nl (F. Messali), J.G.Rots@tudelft.nl (J.G. Rots), daniela.addessi@uniroma1.it (D. Addessi), stefano.pampanin@uniroma1.it (S. Pampanin).

https://doi.org/10.1016/j.engstruct.2022.114078
Received 17 September 2021; Received in revised form 5 February 2022; Accepted 26 February 2022
Available online 20 March 2022

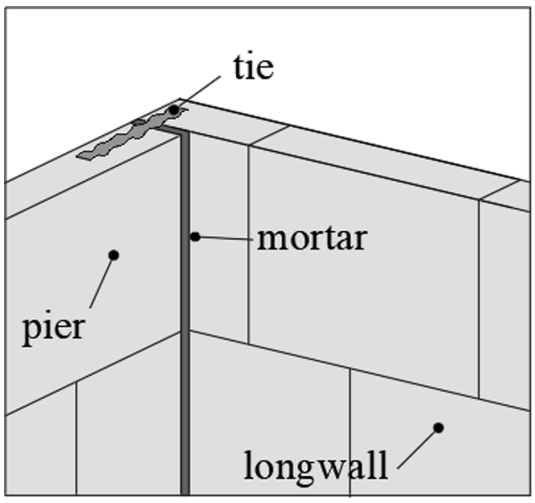

Fig. 1. Pier-main wall system with calcium silicate elements and continuous vertical joint.

test demonstrated that the shear failure of the connection causes a sudden and not negligible loss of bearing capacity of the structure.

The behaviour of low-rise structures with loadbearing walls made of calcium silicate masonry was also studied for the Esecmase project at both wall [3,4] and building [5] level. Namely, calcium silicate blocks were used among other masonry units, whose dimensions in between bricks and units usually require the presence of a continuous vertical joint at the wall intersections.

After 2014, due to the increase of gas-extraction induced seismicity in the Netherlands, a research program was started to assess the vulnerability of typical Dutch URM buildings in several laboratories, among which the MacroLab/Stevin laboratory of Delft University of Technology. Two full-scale masonry assemblages representative of the loadbearing structure of a typical two-storey terraced house were tested in quasi-static cyclic test in 2015 and 2016 [6,7]. Since then, several numerical simulations were conducted to compare the numerical results to the experimental tests [7-9]. The seismic response of buildings made of calcium silicate masonry has been studied in recent years also via shaking table tests at the laboratory of Eucentre [10,11] and LNEC [12], while specific studies of the out-of-plane performance of U-shaped sub-assemblies was investigated in [13-15].

In recent years, many procedures and methods were developed to accurately model the response of URM structures under seismic loads [16-21]. These can be classified according to different criteria. One of the most used classifications distinguishes between the different modelling scales [18,22], namely micromechanical, macromechanical and multiscale approaches. Micromechanical models accurately describe masonry considering all the geometrical details and mechanical response of each constituent, bricks/blocks, mortar and eventually interfaces between them [20,23-27]. Macromechanical models consider masonry as an equivalent homogenized material and adopt phenomenological constitutive laws often based on damage, smeared crack/crush and plasticity formulations [28-33]. These are less computationally demanding as opposed to micromechanical approaches and can be adopted to describe global aspects of masonry response, with localized as well as diffused distributions of damage and cracking. Multiscale procedures are the most modern modelling approach for composite heterogeneous materials like masonry, representing a fair compromise between accuracy and computational costs [34-37]. Also simplified macro-models have been widely proposed, as those based on the equivalent frame approach, which use a single 1D, 2D or 3D macro-element for each pier and spandrel composing the masonry wall [38-43].

Commonly, all the aforementioned modelling approaches are implemented in a finite element (FE) framework adopting 1D beam, 2D solid, plate and shell, or 3D solid formulations, with proper constitutive laws describing the main nonlinear mechanisms occurring in masonry.

This paper investigates the numerical response of masonry assemblages experimentally tested under quasi-static cyclic loading, particularly focusing on the modelling of thin layer mortar joints. Both micro and macromechanical approaches are explored adopting different constitutive laws for masonry, also to study the response of the continuous vertical joints and their effect on the masonry assemblage behaviour. In particular, a full-scale specimen, representing the loadbearing structure of a typical Dutch two-storey masonry building built in the period 1960–1980, is analyzed, typically comprising small CS bricks and running bond pattern. This choice was aimed to validate the use of the proposed modelling approaches for masonry and continuous connections.

The software DIANA FEA 10.2 [44] was used to perform the numerical analyses validated against the experimental outcomes. Also, issues concerning convergence properties and stability of the numerical results are discussed.

Section 2 introduces the different constitutive models adopted in this study for describing masonry and the thin layer mortar joint. Section 3 presents the results of the numerical simulations performed on one of the two-storey masonry assemblages tested at TU Delft in 2015 [6], as well as the comparison with the experimental results. In Section 4, the appropriate modelling of the continuous vertical connection is analyzed first at the component level, by comparing the results to the experimental wall/pier component tests conducted by Raijmakers and Van der Pluijm [2]. Then, the problem is upscaled to the structural level, adding the continuous vertical joint in the full-scale two-storey models already presented in Section 3. The final remarks are reported in Section 5.

2. FE modelling approaches for masonry

Among the alternative approaches proposed to model nonlinear masonry structural response, attention is herein focused on macro and micromechanical finite element procedures. These are distinguished for

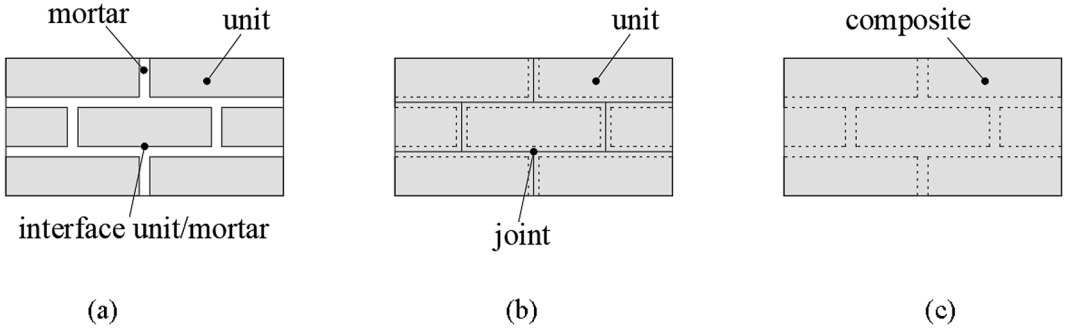

Fig. 2. Modelling strategies for masonry structures: (a) detailed micromodelling, (b) simplified micromodelling, (c) macromodelling [20].

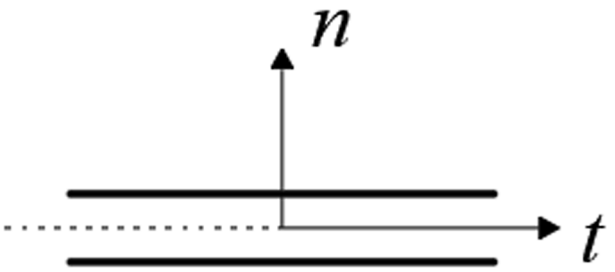

Fig. 3. Intrinsic referenced system of interface element: normal direction for Mode I, tensile cracking - compression crushing, and tangential direction for Mode II.

the scale and detail of the modelling. Micromodelling usually provides the most accurate numerical description of the structure, where mortar joints and units are modelled separately accounting for all the details about geometry and arrangement. This approach is mainly used for the analysis of small components, where the response strongly depends on the interaction and local distribution of stresses between bricks and mortar. A simplified and less cumbersome micromodelling procedure considers the unit-mortar interfaces and the mortar as a single interface or continuous element, while the bricks are represented as a continuum. For numerical analysis of real-scale masonry structures, micromodelling is usually computationally too demanding, and macromechanical approaches are often preferred. The latter methods consider masonry as a homogenized continuum material where a phenomenological constitutive law is introduced, and the local stress and strain distributions are smeared out. Fig. 2 shows different approaches to model masonry structures as reported in literature [20].

This paper adopts two different strategies to describe the crack propagation in the framework of micro and macromodelling approaches for masonry structures, namely discrete and smeared cracking models [45].

The discrete model concentrates the material nonlinear mechanisms (cracking and sliding) in interface elements separating two continuous elements. The constitutive law for the interface elements is defined in terms of normal/shear forces and relative displacements, according to the displacement discontinuity occurring in the fractures. Before the development of the crack, the stiffness of the interface element is usually defined a sufficiently high dummy value so as to make the initial deformation of the interface negligible compared to the initial deformation of the bulk material. The behaviour during the softening phase, i.e. when cracking or sliding occurs, is described by the following relation [45]:

$$\mathbf{t}^{cr} = \mathbf{C}^{cr}\mathbf{s}^{cr} \tag{1}$$

where $\mathbf{t}^{cr} = [t_n\ t_t]^T$ and $\mathbf{s}^{cr} = [s_n\ s_t]^T$ are the traction vector and relative displacement across the crack, respectively. Both vectors have components in the normal, '*n*', and tangential, '*t*', direction of the interface, as illustrated in Fig. 3. The matrix $\mathbf{C}^{cr}$ describes the adopted nonlinear constitutive law considering a tensile cracking and compression crushing in normal direction (Mode I) and shear sliding in tangential direction (Mode II). The use of discrete interfaces reflects the real nature of the displacement discontinuity of the crack but results as not convenient in the framework of the finite element displacement method [45]. An additional drawback of the discrete approach is the need to know a priori where the crack may develop [1].

In the smeared crack approach, the crack is spread out over the finite element, modelling the cracked material as a continuum. The nonlinear behaviour is described through stress–strain relations, which do not fit to the real displacement discontinuity of the fracture but are computationally less demanding [45]. Unlike the discrete models, the crack may occur at any location and direction, allowing to solve structural problems where the position of the crack is initially unknown. The

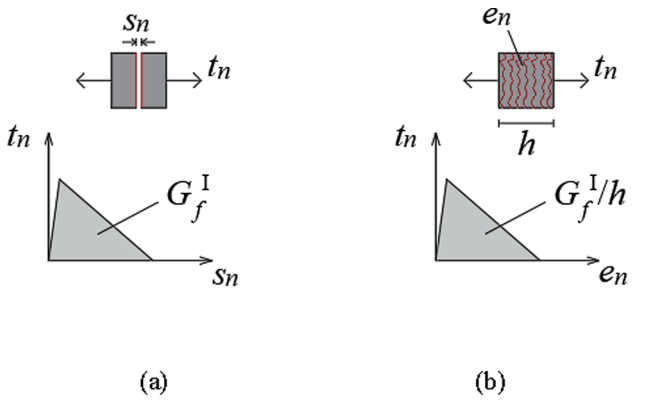

Fig. 4. Constitutive law for Mode I: (a) discrete and (b) smeared crack models.

formulation of the smeared cracked models is usually based on the decomposition of the total strain $\boldsymbol{\varepsilon}$ in two components, the strain occurring in the crack $\boldsymbol{\varepsilon}^{cr}$ and that in the continuum material between the cracks $\boldsymbol{\varepsilon}^{co}$ [45]:

$$\varepsilon = \varepsilon^{cr} + \varepsilon^{co} \tag{2}$$

The strain in the crack $\boldsymbol{\varepsilon}^{cr}$ is expressed by the strain in its local reference system $\mathbf{e}^{cr}$, i.e. the normal and tangential direction '*n*' and '*t*', using the transformation matrix **N**, accounting for the orientation of the crack. This method allows to develop the fixed single, fixed multi-directional and rotating crack model, and properly evaluate the redistribution of the rotated principal stresses after the crack [45]. The nonlinear constitutive law for the crack is governed by the matrix $\mathbf{D}^{cr}$, which allows to introduce Mode I, Mode II, and, if selected, mixed-Mode components and is expressed as:

$$\mathbf{t}^{cr} = \mathbf{D}^{cr}\mathbf{e}^{cr} \tag{3}$$

where $\mathbf{t}^{cr}$ and $\mathbf{e}^{cr}$ denote the traction and strain vectors expressed in the intrinsic local reference system of the crack. In these decomposed-strain based smeared crack models the behaviour of the smeared crack is decoupled from the behaviour of the bulk material, which is usually treated as linearly elastic, thus obtaining an elastic-softening description for the smeared cracked continuum. Alternatively, total-strain based stress–strain relations can be used which describe the behaviour of concrete and masonry in a more direct and engineering way, e.g. [49].

Fig. 4 shows the constitutive law for Mode I in the case of the (a) discrete and (b) smeared approach characterized by a linear softening branch. In the discrete approach, as previously mentioned, the constitutive law is expressed in terms of traction and relative displacement and the slope of the softening branch is ruled by the fracture energy G_f^I. Instead, in the smeared crack approach, the nonlinear behaviour is defined by a stress–strain relation, which depends on the fracture energy divided by the so-called crack bandwidth *h*, which is a function of size, shape and interpolation functions of the finite element. For linear two-dimensional elements, *h* may be assumed equal to $(2A)^{1/2}$, and for higher order two-dimensional elements equal to $(A)^{1/2}$, where *A* is the total area of the element. In case of solid element, the crack bandwidth may be calculated with $h = (V)^{1/3}$, where *V* is the volume of the element [44].

2.1. Constitutive laws used to simulate continuous vertical joints

The behaviour of continuous vertical pier-wall connections at the corner of URM buildings is simulated in this work by means of interface elements. The failure criterion for the interface includes both discrete cracking for tension and discrete sliding for shear.

The tensile failure is ruled by the normal traction versus normal relative displacement law, defined by two mechanical parameters, the tensile strength f_t and the Mode I fracture energy G_f^I. Different shapes of

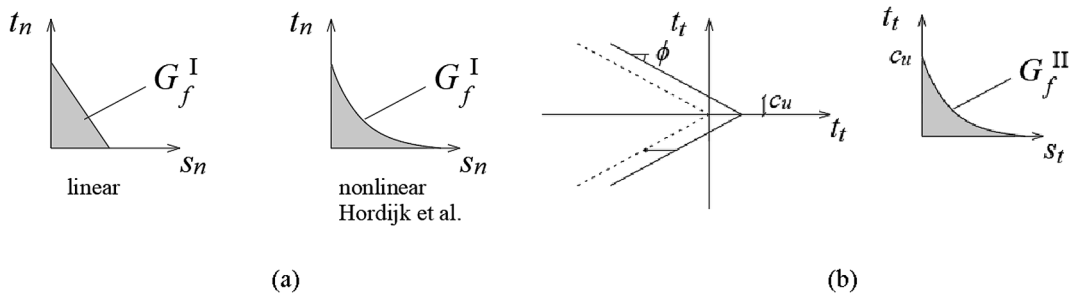

Fig. 5. Constitutive laws for interface element: (a) Mode I normal traction-relative displacement laws [44]; (b) Coulomb friction model for shear stresses and Mode II shear traction-relative displacement law [1].

the softening branches can be considered as shown in Fig. 5**(a)**. For the sliding shear failure, the plasticity based Coulomb friction model is adopted, which depends on the cohesion c_u and friction angle ϕ. The Coulomb yield limit function is defined as:

$$|t_t| \leq c_u - t_n \tan\phi \tag{4}$$

As shown in Fig. 5**(b)**, cohesion softening has been included, defined by an exponential shear softening diagram and the Mode II fracture energy G_f^{II}. When the Mode II softening is completed, the criterion reduces to dry friction, as indicated by the dashed line in Fig. 5(b). Either associated or non-associated plasticity were used. In the former case the dilatancy angle, defining the uplift upon shearing, is equal to the friction angle, whereas in the latter case it is lower than the friction angle. Optionally, a compression cap can be added for combinations of shear with high compression, but this was not activated in the present study.

The Coulomb friction model is a plasticity-based formulation with explicit coupling between normal and shear behaviour, requiring return mapping schemes to solve for the elastic and plastic part of the relative displacements. Special treatment is to be considered when the stress point is returned to a discontinuity such as an apex, and non-symmetric stiffness matrices have to be handled in case of non-associated plasticity. This may complicate the analyses, especially when it comes to brittle behaviour of large-scale structures. Therefore, in this study also an alternative and simpler constitutive model has been tested, that is a nonlinear elastic model, where the normal and shear tractions are uncoupled and expressed as a direct function of the corresponding relative displacements only. Thus, the stiffness matrix results diagonal, speeding up the convergence of the numerical analyses [44]. On the other hand, this does not allow to express the shear strength as function of the normal traction at the integration point, which means that a priori estimates or design assumptions for the local shear strengths have to be made. The uniaxial relationships are obtained by multi-linear diagrams defined by the users to simulate properly the normal and shear behaviour of the interface.

$$\begin{bmatrix} t_n \\ t_t \end{bmatrix} = \begin{bmatrix} k_n & 0 \\ 0 & k_t \end{bmatrix} \begin{bmatrix} s_n \\ s_t \end{bmatrix} \tag{5}$$

For example, a multi-linear diagram of the traction-relative displacement for the tangential direction is shown in Fig. 14. In particular, the tangential constitutive law is determined by the maximum shear stress and residual shear strength, which affect the peak and post-peak branch, respectively.

2.2. Constitutive laws for smeared crack models used to simulate masonry

In the framework of the smeared crack modelling, two constitutive formulations are used in this work: a total-strain based crack model with isotropic properties [44,49] and a total-strain based pre-fixed

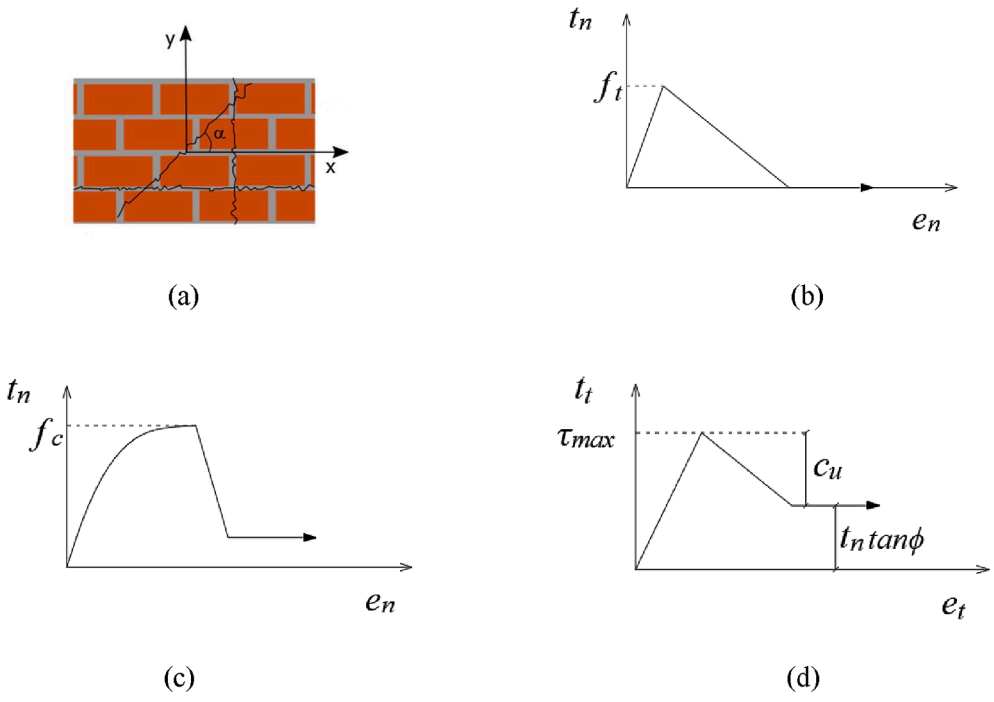

Fig. 6. Engineering Masonry Model (EMM): (a) the angle α for diagonal stair step cracks, (b) cracking, (c) crushing, and (d) chear behaviour [33,46,44].

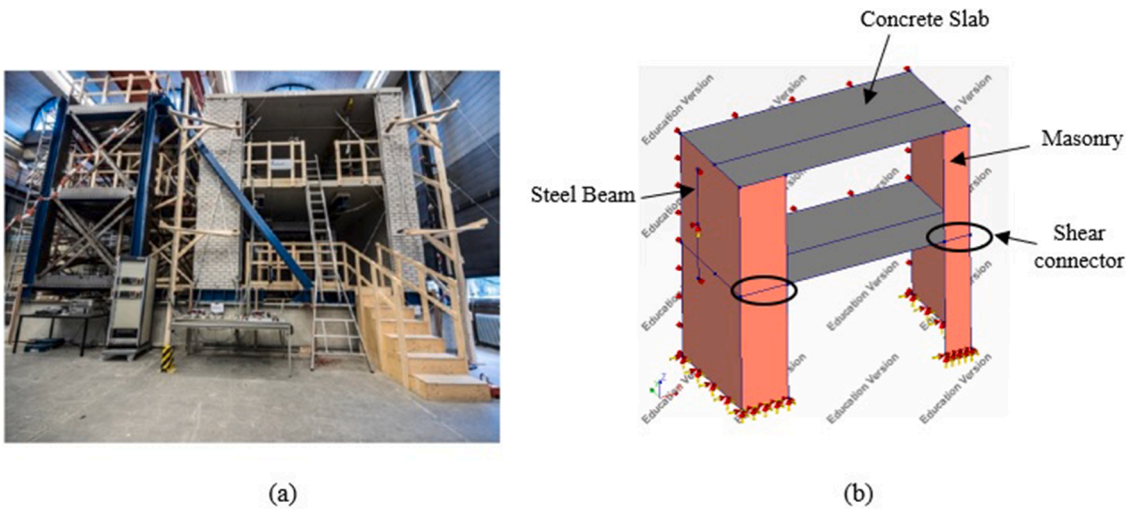

Fig. 7. (a) Specimen and construction detail of a typical two-storey terraced house [3] and (b) simplified modelling schematic.

orthotropic crack model [33,44,46]. The former was initially developed for concrete and assumes isotropic properties for both initial elastic and nonlinear parameters, while the latter was developed as an engineering oriented model with simple assumptions regarding the orthotropy of masonry. In the following, the former will be referred to as TSCM (total-strain crack model) and the latter as EMM (engineering masonry model).

As for the TSCM, two different versions are available referring to the fixed and rotating crack model, respectively. The first defines the stress–strain relation in the fixed directions defined at the onset of cracking, whereas the rotating crack model defines the stress–strain law in the continuously rotating principal strain directions. The fixed crack model uses an explicit shear retention factor or function to reduce the shear stiffness after cracking, while the rotating crack model can be considered to include an implicit shear term that guarantees coaxiality between principal stresses and strains [45]. In this study, the rotating version of the TSCM was adopted. Various functions are used to describe the softening branch for tension and compression, governed by the tensile and compression fracture energy, respectively.

The idealization of masonry as an isotropic material, despite its anisotropic nature, and the lack of distinction between the shear and tensile failure are two relevant shortcomings of the TSCM, when used for masonry. Additionally, the secant unloading/reloading formulation adopted for TSMC largely underestimates the energy dissipation under cyclic loads, when shear failure occurs.

The EMM was developed to specifically model the nonlinear behaviour of masonry, overcoming the abovementioned drawbacks of the TSCM [33,47]. In particular, the distinction between different failure modes and the use of a bilinear unloading/reloading path (which consists of a succession of an elastic and a secant branch) returns a more realistic energy dissipation under cyclic loads. In addition, the EMM considers the anisotropy of the masonry distinguishing between the different stiffness, strength and softening properties in the directions parallel to the bed- and head-joints, respectively. Additionally, the tensile cracks may occur in only three predefined directions: normal to the bed- and head-joint directions and along the diagonal stair step cracks defined by the angle α (Fig. 6 (a)). The uniaxial tensile and compressive behaviour is defined by the relation between the stress t_n and strain e_n in the normal direction, governed by the tensile and compression fracture energy. A linear softening branch is adopted in tension (Fig. 6 (b)), whereas the curve in compression is defined via a sequence of a third order curve and a parabolic curve up to the compressive peak, f_c, and a linear softening branch up to a residual stress

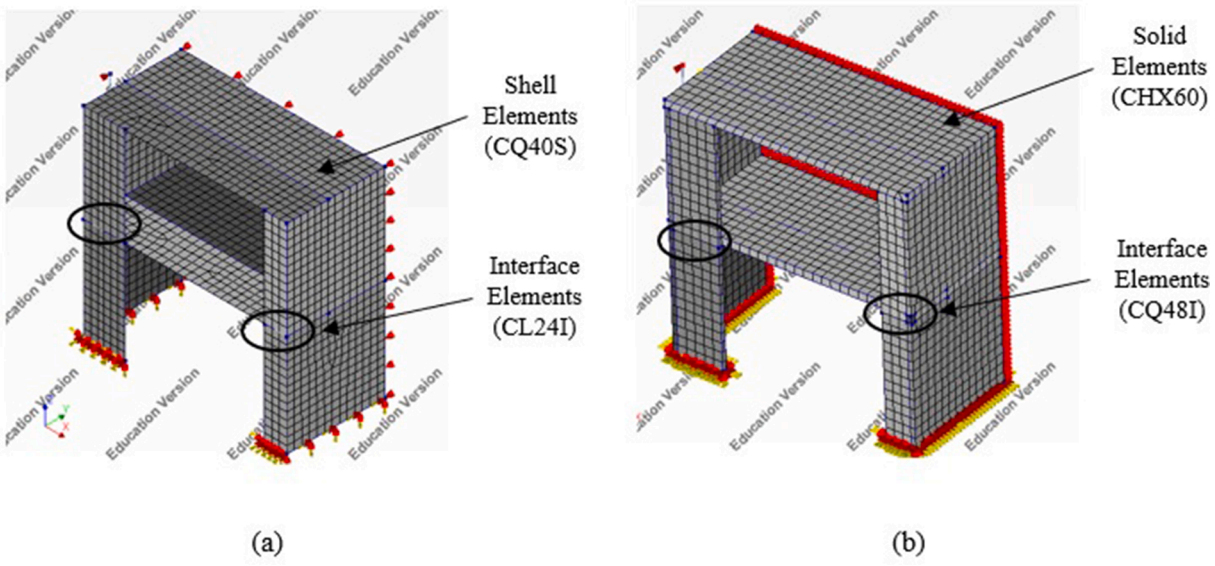

Fig. 8. Mesh made of shell (a) and solid (b) elements.

Table 1
Total Strain Crack Model: mechanical parameters.

Mechanical Parameters		Values	Units	Standard
Elastic modulus	E	3264	MPa	EN1052-1
Poisson ratio	ν	0.16		*
Shear modulus	G	1306	MPa	*
Mass density	ρ	1805	kg/m^3	–
Tensile strength	f_t	0.19	MPa	EN1052-5
Tensile fracture energy	G_f^I	0.0127	N/mm	*
Compression strength	f_c	5.8	MPa	EN1052-1
Fracture energy in compression	G_{fc}^I	17.4	N/mm	*

* value not available from material testing and assumed based on the literature.

Table 2
Engineering Masonry Model: mechanical parameters.

Mechanical Parameters		Values	Units	Standard
Elastic modulus perpendicular to head joint	E_x	2212	MPa	EN1052-1
Elastic modulus perpendicular to bed joint	E_y	3264	MPa	EN1052-1
Shear modulus	G	1306	MPa	*
Mass density	ρ	1805	kg/m^3	–
Tensile strength normal to bed joint	f_{ty}	0.19	MPa	EN1052-5
Minimum strength head-joint	f_{tx}	0.38	MPa	*
Tensile fracture energy	G_{ft}	0.0127	N/mm	*
Angle between stepped diagonal crack and bed joint	θ	0.792	rad	–
Compression strength	f_c	5.8	MPa	EN1052-1
Fracture energy in compression	G_{fc}	17.4	N/mm	*
Factor to strain at compressive strength	n	5	–	*
Unloading factor for compression	λ	0	–	*
Friction angle	γ	0.406	rad	EN1052-3
Cohesion	f_{vo}	0.14	MPa	EN1052-3

* value not available from material testing and assumed based on the literature.

equal to 10% of the compressive strength (Fig. 6 (c)). The shear behaviour is described by the Coulomb friction model, with the post-peak behaviour governed by Mode II fracture energy. In particular, the in-plane shear stress t_t is computed based on the in-plane shear strain e_t, and the stress t_n in the direction normal to the bed-joint (Fig. 6 (d)) [33,46].

3. Modelling of a masonry structure with strong connections

This section describes the numerical modelling of the first (out of two) two-storey masonry assemblages tested at TU Delft in 2015 [6,7]. The full-scale specimen, shown in Fig. 7 (a), represents the loadbearing structure of a typical Dutch two-storey masonry building built in the period 1960–1980, typically comprising small CS bricks and running bond pattern.

A schematic view of the masonry modelling is illustrated in Fig. 7 (b). Considering geometry and loading scheme, providing symmetry conditions, only half structure was modelled to reduce the computational effort. This is a convenient modelling assumption, although symmetry could be partially lost as a consequence of the damage evolution and localization.

To further simplify the numerical model, piers and walls were considered to be fixed at the base, thus neglecting any deformation of the steel substructure. Continuity condition was assumed for the connection between the slab of the second floor and the walls and piers. Conversely, the weight of the first floor is carried only by the wall. More specifically, the concrete slab is connected to the piers by anchors, which prevent their out-of-plane deflection. The behaviour of the anchors was simulated via interface elements with non-zero stiffness in the out-of-plane direction of the pier. A quasi-static cyclic loading regime was applied to the structure through two couples of actuators coupled so that equal forces were applied at the two floors. In the numerical model, a displacement-controlled monotonic pushover analysis was performed and a fictitious rigid steel beam with appropriate restraints was added to enable the analysis to be steered in displacement-control, simulating the experimental loading conditions. It is worth mentioning that the monotonic pushover analysis is a simplified simulation of the experiment, neglecting the effects of the quasi-static cyclic load, such as the cumulative damage of the masonry.

Three numerical models were developed to investigate the effect of the adoption of different constitutive laws (TSCM and EMM) and element types (shell and solid) on the outcomes of the simulation. Since the EMM was not yet implemented for solid elements, the following models were analyzed: TSCM-Shell model, TSCM-Solid model, EMM-Shell model. The adopted meshes comprising shell and solid elements are shown in Fig. 8. For the shell models, quadratic 8-node elements, CQ40S, were used, with a reduced 2x2 Gauss integration scheme and a mesh size of approximately 200 mm. The thickness of the elements is equal to the depth of the bricks and seven integration points were used along the thickness to obtain a good interpolation for the out-of-plane behaviour of the walls. The interfaces which connect the piers and the floor at the first storey level were modelled using interface elements between curved shell elements, CL24I, with quadratic interpolation and 3-point Newton-Cotes integration scheme along the longitudinal direction, and 3-point Simpson scheme along the thickness. For the 3D solid models, quadratic 20-node solid brick elements, CHX60, were used for the model in Fig. 8 (b), with full Gauss (3x3x3) integration scheme. Quadratic 2D plane interface elements, CQ48I, with quadratic interpolation and 3x3 Newton-Cotes integration scheme were used in this model.

Most of the adopted material parameters were derived from the values of the experimental companion tests performed at material level, as described in [6] and [7]. Those not available were set according to the relations in literature, as specified below.

The parameters introduced in the TSCM are summarized in Table 1. A rotating crack model with linear (in tension) and parabolic (in compression) fracture-based softening curves were adopted. The crack bandwidth of the elements was assumed according to proposal by Rots [44]. Since in this model the material is considered to be isotropic, the elastic modulus was selected equal to that perpendicular to the bed joints. For the Poisson ratio, a typical value for the masonry was assumed equal to 0.16 (corresponding to a ratio between the shear and Young's modulus equal to 0.43). The value of the tensile strength was computed as 2/3 of the flexural strength of masonry, and the Mode I fracture energy G_f^I was calculated through the relation [46]:

$$G_f^I = 0.025(2f_t)^{0.7} \tag{6}$$

The compressive fracture energy is provided by the following formula [46]:

$$G_{fc}^I = 15 + 0.43f_c - 0.0036{f_c}^2 \tag{7}$$

The mechanical parameters adopted for the EMM are reported in Table 2. This model accounts for the material anisotropy both in the linear elastic and nonlinear stage. The Young's moduli for both the direction perpendicular to the bed and head joints were derived from the experimental companion tests. The minimum tensile strength normal to the head joint was calculated as $f_{tx} = 2\,f_{ty}$ [46]. The angle between the diagonal crack and the bed joint, depending on the brick size, was approximately computed as $2h_b/l_b$, being h_b and l_b the height and length of the brick, respectively. Secant unloading for tension, elastic

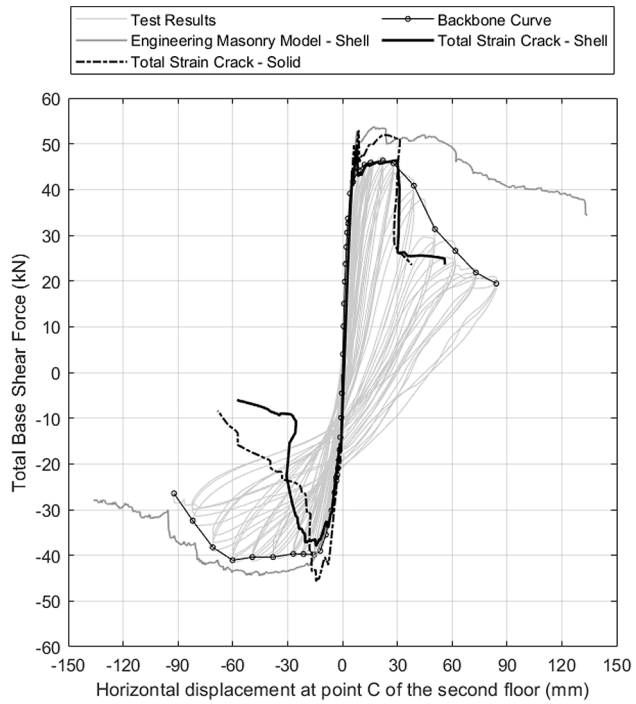

Fig. 9. Comparison of the capacity curves: experimental results (thin grey solid line), EMM-Shell (tick grey solid line), TSCM-Solid (dashed-point black line) and TSCM-Shell (black solid line).

unloading for shear and elastic unloading for compression were assumed.

Pushover analyses were performed by first applying the gravity loads, and then monotonically increasing the displacement applied to the middle point of the rigid steel beam up to a maximum value of ± 100 mm, in both the positive and negative direction. An incremental-iterative procedure was used with the classical Newton-Raphson algorithm to solve the nonlinear problem.

Fig. 9 shows a comparison between the results obtained using the three different numerical models (EMM-Shell, TSCM-Shell, TSCM-Solid) and the backbone curve of the experimental test (reported in [3]). Overall, all models correctly reproduce the initial elastic branch. The models also predict similar values of the peak strength, although all overestimate the experimental value in the positive direction. Small differences are observed for the TSCM-Solid model, which reaches a slightly larger limit strength for the negative loading direction. However, the differences at peak between TSCM-Shell and TSCM-Solid models are overall very limited. The numerical results depart in the post-peak phase. In particular, in case of TSCM, the capacity curve suddenly decreases showing a brittle failure, whereas the EMM shows a more gradual strength degradation. The differences emerging in the post-peak branch are related to the different failure mechanisms predicted. In particular, the gradual loss of capacity for the EMM is caused by the progressive toe-crushing of the wide pier (Fig. 10 (b)), while the sudden drop of the capacity occurring for the TSCM is due to the diagonal cracking of the same wide pier (Fig. 10 (c) and (d)). The latter failure mechanism corresponds to that observed during the experimental test (Fig. 10 (a)), although the numerical post-peak softening for the TSCM is more brittle than that of the experimental backbone curve. In conclusion, the selection of the constitutive law clearly affects the type of failure mechanism developed and thus strongly influences the global response of the structure. Additionally, the results show that the use of solid or shell elements influences only the peak strength, and not the occurring failure mechanism.

4. Continuous vertical joints in masonry assemblage

As anticipated, typical Dutch URM structures built after 1980 are characterized by the use of Calcium Silicate (CS) elements, with the piers connected to the transversal walls through continuous vertical connections. The continuous thin layer mortar joints was made of cement-based mortar with high compressive strength and limited thickness (2–3 mm), and no steel ties were present. These ties were able to provide an efficient tensile restraint, but they did not have any significant shear stiffness due to the limited thickness and were not able to prevent or postpone significantly the shear failure along the joint. A common modelling approach considers the interlocking of the masonry brick as a rigid connection, but in case of a continuous joint, this approach may overestimate the seismic capacity of the structure. Specifically, the seismic performance may be strongly reduced by the shear failure of continuous vertical connections, as shown by the experimental campaign performed by Raijmakers and Van der Pluijm [2], who analyzed the failure mechanism of a masonry U-shaped assemblage under lateral load. Here, the numerical modelling of the continuous vertical joint is discussed, first at the element structural level, considering a U-shaped assemblage tested by Raijmakers and Van der Pluijm, and then at the full structural level, by including a thin layer mortar joint in the models of the full-scale two-storey building tested at TU Delft and described in the previous section.

4.1. Modelling of the vertical joint in a U-shape assemblage

This section aims to analyze the numerical modelling of a thin layer mortar joint, comparing it with the results of the experimental test conducted by Raijmakers and Van der Pluijm [2]. The specimen was composed of calcium silicate units and continuous vertical joints between the main wall and the piers. The schematic of the test is shown in Fig. 11. A monotonically increasing horizontal load was applied at the top of the wall, along with the vertical load, which was maintained constant during the test and contributes, together with the self-weight of the components, to the stabilizing moment of the structure.

The results of the experimental campaign show three types of possible failure mechanisms. The rocking of the entire assemblage Fig. 12 (a) consists of the ideal tilting of the whole structure around the toe of the pier. A typical mechanism in case of toothed connection is the diagonal cracking/compression failure of the pier (Fig. 12 (b)). This mechanism reduces the capacity curve as illustrated in Fig. 12, preventing the full development of the rocking mechanism. The shear failure of the wall-pier connection Fig. 12 (c) may occur for weaker connection types, as for the thin layer mortar joints. In this case, the brittle failure of the connection determines a sudden reduction of the strength of the U-shape assemblage prior to the pier failure [1].

To properly describe the behaviour of the continuous vertical joint, nonlinear interface elements were adopted to simulate the shear failure of the connection. However, the brittle failure of the joint may lead to instability of the numerical analysis. In the following, the two constitutive laws described in Section 2.1 are compared: the Coulomb friction model and the Nonlinear Elastic model. Two different finite element models are also considered and shown in Fig. 13: a two-dimensional (2D) and a three-dimensional mesh (3D), which use plane stress or solid elements, respectively. In the two-dimensional model, 4-node quadrilateral isoparametric elements, Q8MEM, with the mesh size equal to 100 mm were used. Bi-linear interpolation functions were then adopted for the displacement fields, together with a 2x2 Gauss integration scheme. For compatibility, L8IF interface elements with linear interpolation were selected to model the connections. In the three-dimensional model, the pier and main wall were modelled with 8-node isoparametric solid brick elements, HX24L, with tri-linear interpolation for the displacements and 2x2x2 Gauss integration scheme. The mesh size was equal to 100 mm. The connections were modelled through Q24IF interface elements based on linear interpolation. As

(a)

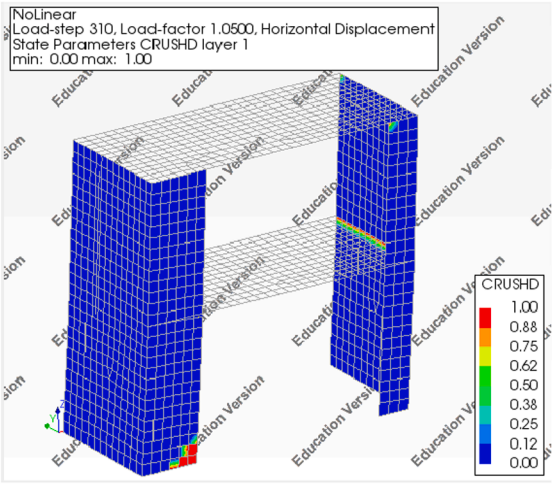

(b)

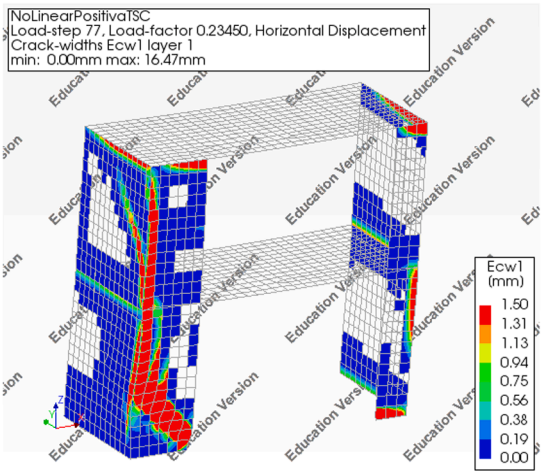

(c)

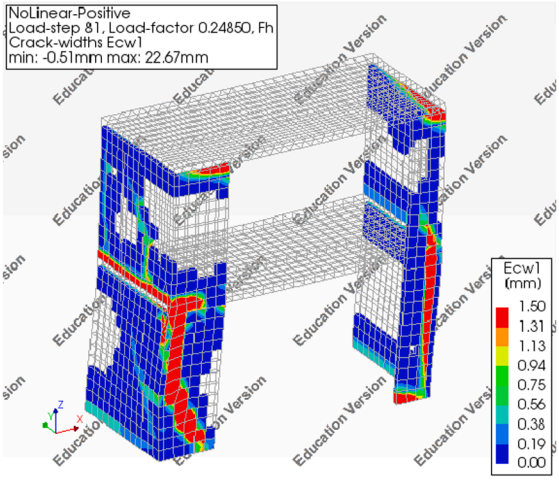

(d)

Fig. 10. Failure mechanism for each model: (a) Experimental test (diagonal cracking) [5], (b) EMM Shell model (toe-crushing), (c) TSCM Shell model (diagonal cracking) and (d) TSCM Solid model (diagonal cracking).

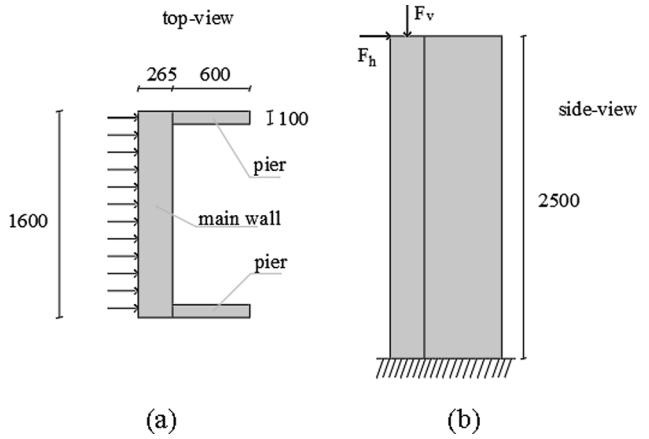

Fig. 11. Piers-main wall connection (Raijmakers and Van der Pluijm [1]): (a) geometry and (b) loading conditions.

suggested in literature [1], the Calcium Silicate masonry was assumed to behave linearly elastically. Boundary interface elements with no-tension behaviour were introduced at the base of the masonry elements. A displacement-controlled analysis was performed by applying a prescribed displacement to the node at the top of the wall, as illustrated in Fig. 13.

The material parameters adopted for masonry and interface elements modelled through the Coulomb friction model are summarized in Table 3, set according to the numerical simulation performed by Rots [1]:

The Nonlinear Elastic constitutive law, as mentioned before, assumes an uncoupled behaviour in the normal and shear directions of the interface elements. A linear elastic behaviour was considered in the normal direction, which corresponds to the assumption of no opening of the joint. Since the shear strength cannot be expressed as function of the normal traction and a constant normal stress distribution along the interface was assumed, the parameters governing the Nonlinear Elastic constitutive law required a proper calibration.

The traction-relative displacement diagram for the tangential

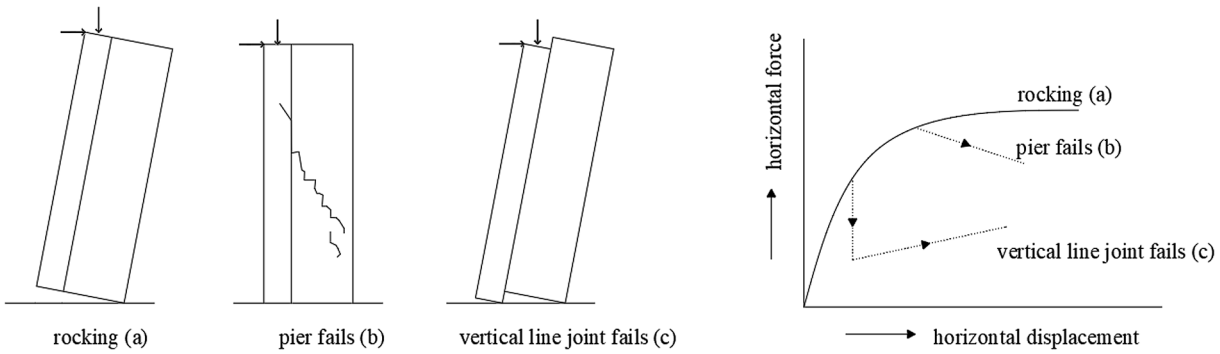

Fig. 12. Possible failure mechanisms of a U-Shaped wall as shown in [1].

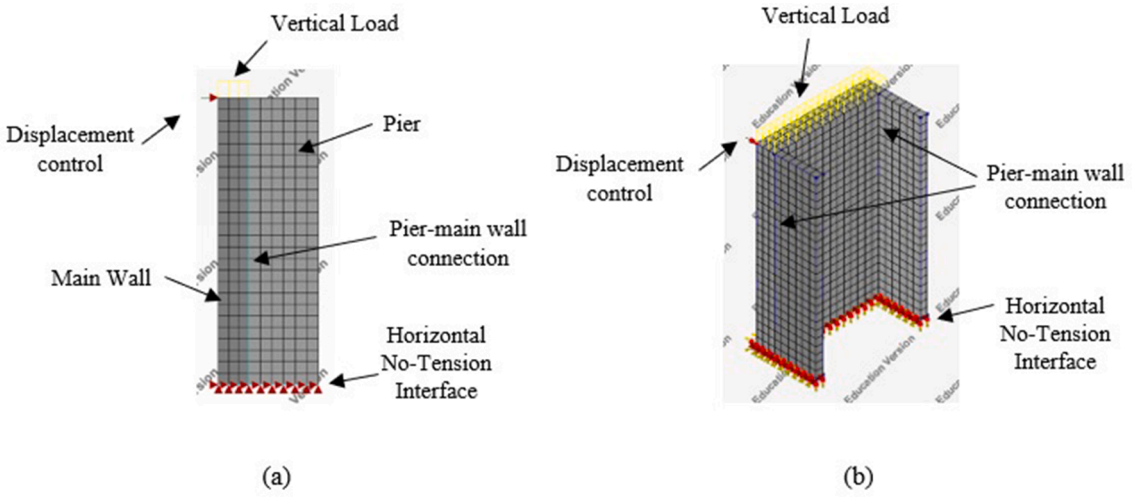

Fig. 13. Model of the U-shape assemblage in DIANA FEA: (a) 2D plane stress and (b) 3D solid model.

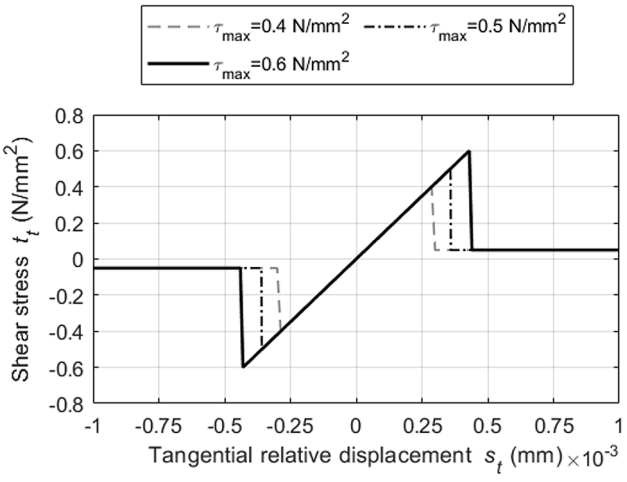

Fig. 14. Shear stress-tangential relative displacement diagram for different maximum shear stress values.

direction is shown in Fig. 14, and presents a brittle failure after the maximum shear stress is achieved. Three values were considered for the maximum shear stress: $\tau_{max} = 0.4$ N/mm^2, 0.5 N/mm^2, 0.6 N/mm^2. The elastic stiffness in tangential direction was taken the same as for the analysis performed with the Coulomb friction failure criterion. A small residual shear strength was considered to simulate the friction of the interface after the sliding. Its value equal to 0.05 N/mm^2 was calibrated to obtain the post-peak branch.

Table 3
U-shape assemblage: masonry and interface Coulomb friction model parameters.

Elements	Mechanical Parameters		Values	Units
Masonry Calcium Silicate (Linear Elastic)	Elastic modulus	E	5000	MPa
	Poisson's ratio	υ	0.12	–
	Shear modulus	G	2232	MPa
	Unit mass	ρ	1800	kg/m^3
Vertical Joint (Coulomb Friction)	Normal stiffness	k_n	3125	MPa
	Shear stiffness	k_t	1395	MPa
	Mode II fracture energy	G_f^{II}	0.05	J/m^2
	Cohesion	c_u	0.4	N/mm^2
	Angle of friction	$tan\varphi$	0.75	–
	Angle of dilatancy	$tan\psi$	0.1	–

The pushover response curves of the U-shape assemblage with the vertical connection modelled by adopting the Coulomb friction or the Nonlinear Elastic constitutive law for the interfaces are reported in Fig. 15 (a) and (b), respectively. The vertical and horizontal axes represent the total shear reaction at the base of the wall and the horizontal displacement in x-direction applied to the node at the top of the wall, respectively. The results are compared with those obtained by Rots in [1], where a load-controlled analysis with a special arc-length method, using crack mouth sliding degrees-of-freedom in combination with true negative tangent stiffness, allowed to accurately describe the snap-back of the capacity curve associated with the propagation of the crack along the interface. The numerical analyses performed in this study pointed out the difficulty in following the post-peak response stage and the computational effort required to reach the convergence of the

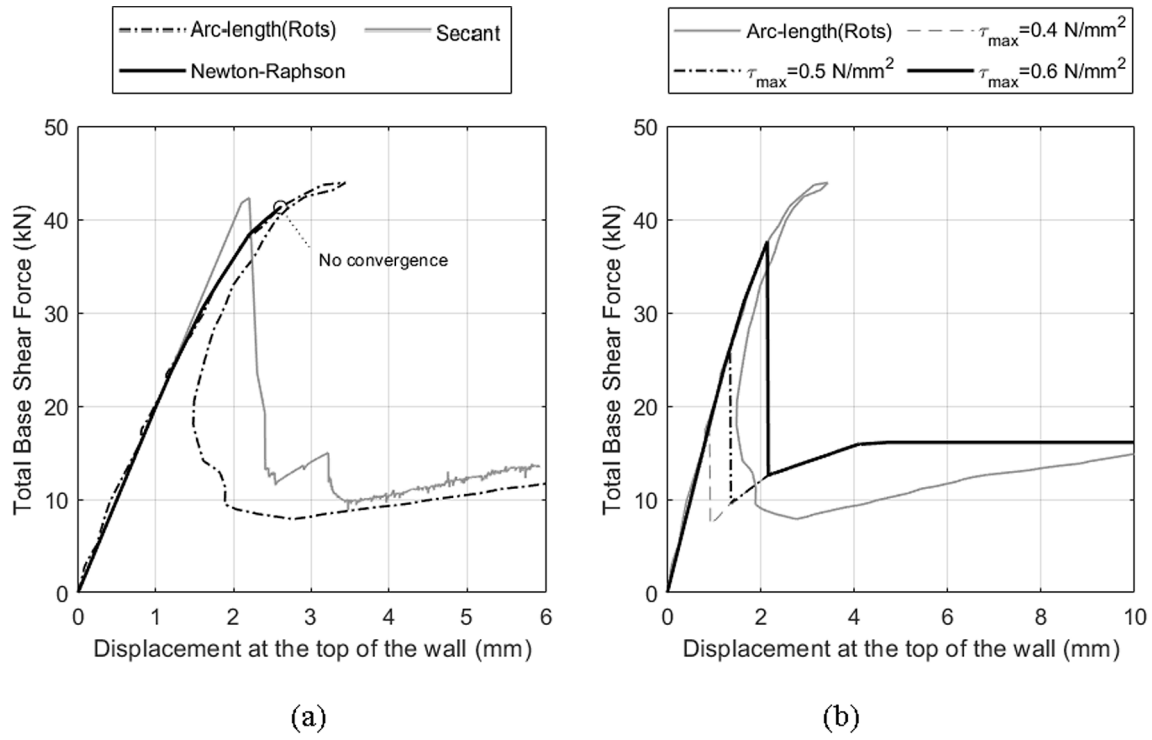

Fig. 15. 2D model capacity curves: (a) Coulomb Friction vs (b) Nonlinear Elastic model as constitutive law for the vertical interface.

solution. In particular, the analysis performed using the Coulomb friction interfaces converges until the onset of the shear failure of the vertical connection. After that, the sudden propagation of the crack along the joint causes the instability of the numerical solution. Specifically, the analyses performed with the Newton-Raphson iterative method diverge after the peak is achieved, whereas those run with the Secant (Quasi-Newton) method describe the post-peak branch, although a very small step size must be set. Besides, the snap-back cannot be described due to the adopted displacement-control, but is "jumped over" by using the Secant Quasi-Newton method.

Unlike the Coulomb-friction model, no convergence issues are observed when the Nonlinear Elastic interfaces are used along with the Newton-Raphson iterative method. The results of the analyses performed by adopting different values of the maximum shear stress are

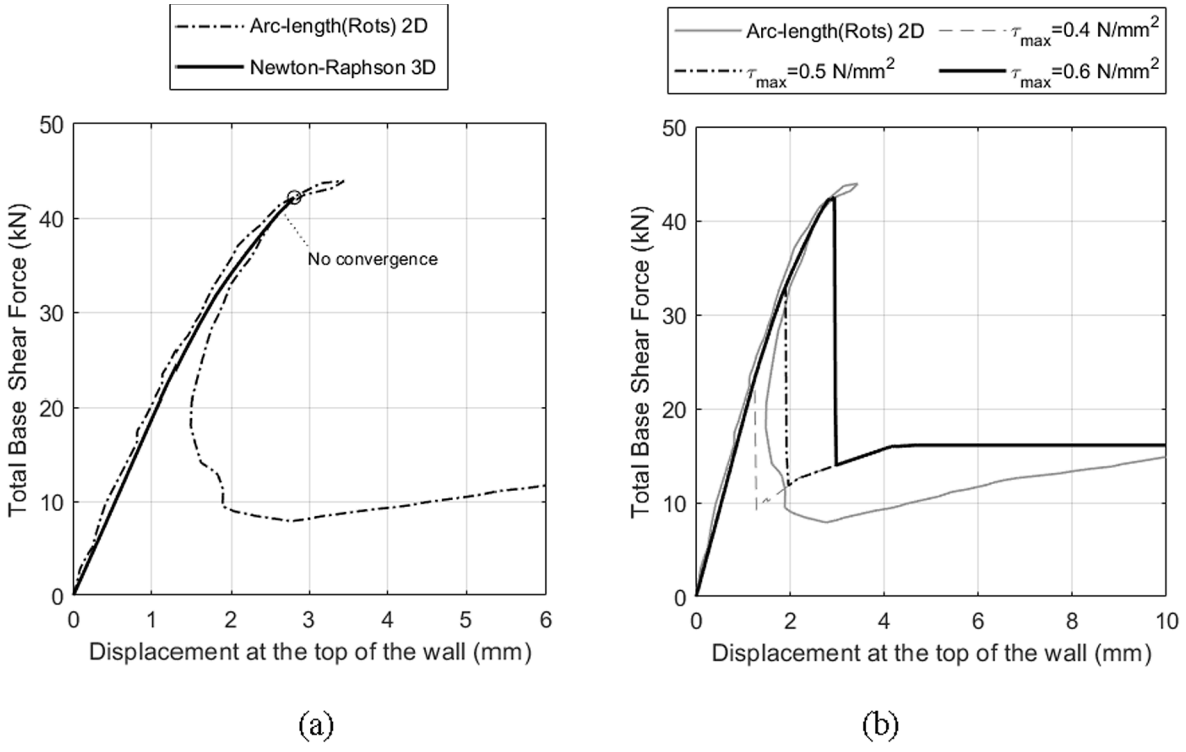

Fig. 16. 3D model capacity curves: (a) Coulomb Friction vs (b) Nonlinear Elastic model as constitutive law for the vertical interface.

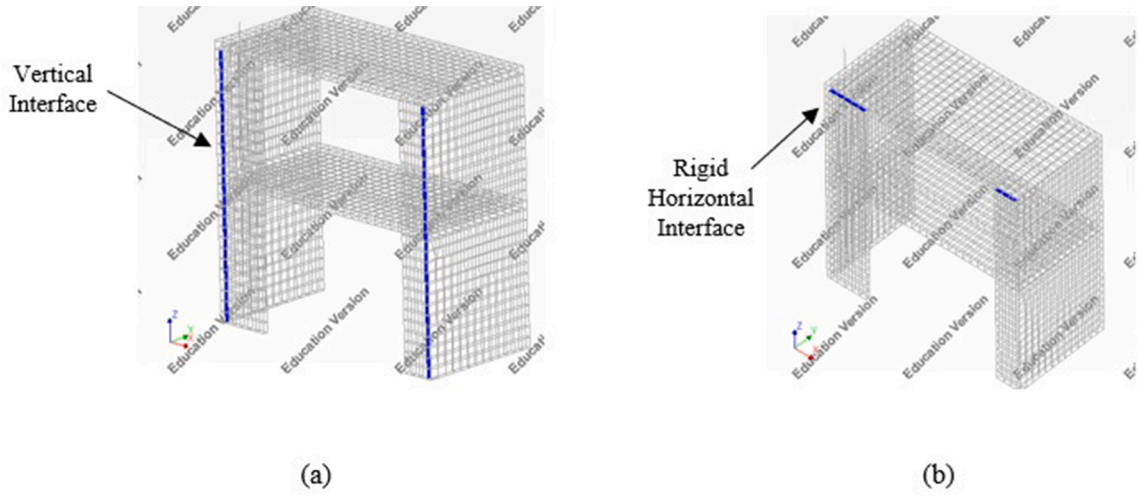

Fig. 17. (a) Vertical interface and (b) rigid horizontal interface.

illustrated in Fig. 15 (b). Once more, as a displacement-controlled analysis was performed, the snap-back cannot be described and the peak load is underestimated for all the cases. Overall, the Coulomb friction-based constitutive law is more adherent to the mechanical behaviour of the joint, but the implemented formulation suffers from numerical instability and hardly allows to describe the post-peak behaviour of the structure. This could be likely related to various issues: the coupled plasticity-based formulation is very sensitive to numerical details in the required return mapping schemes in solving for the elastic and plastic part of the relative displacements; the apex and the combination of Coulomb friction with discrete cracking require special treatment; non-symmetric stiffness matrices in case of non-associated plasticity have to be dealt with. On the other hand, the Nonlinear Elastic interface is a simple alternative to obtain an approximate description of the joint behaviour, although its parameters need to be accurately calibrated to obtain reliable results, for instance considering as a benchmark the outcomes of the testing campaign presented in [15]. The absence of a decomposition of the relative displacements and the straightforward derivation of the tangent or secant stiffness for the independent uniaxial curves obviously make the analysis robust.

Regarding the 3D model, the use of solid elements did not provide a more accurate description of the failure mechanism. On the opposite, this choice presents some drawbacks, such as the much higher computational effort, more convergence problems, or the need to impose the dilatancy angle Ψ equal to the friction angle ϕ to have a symmetric stiffness matrix and increase the robustness of the model. In Fig. 16, the results of the 3D model are compared with those obtained by Rots in [1] for the 2D model.

4.2. *Modelling of the continuous vertical joints in the two-storey masonry assemblage*

The interfaces described in the previous section were used to model the continuous vertical connections between piers and transversal walls in the masonry structure already described and analysed in Section 3.1. The three FE models, TSCM-Shell, TSCM-Solid and EMM-Shell were modified by modelling the discontinuity present along the vertical joints at the corners by means of interface elements, as illustrated in Fig. 17 (a). A rigid horizontal interface between the pier and the second floor was added to allow the sliding along the joints after failure, as shown in Fig. 17 (b).

First, the Coulomb friction constitutive law was adopted for the vertical interfaces. A sensitivity study was performed by varying the value of the friction angle, expressed as a percentage of the initial angle ϕ equal to 0.64 rad (as for the U-shape assemblage). The friction angle was gradually reduced to obtain sliding failure along the interfaces, and Fig. 18 shows the corresponding capacity curves. It was observed that the numerical model is not robust, since the convergence is extremely

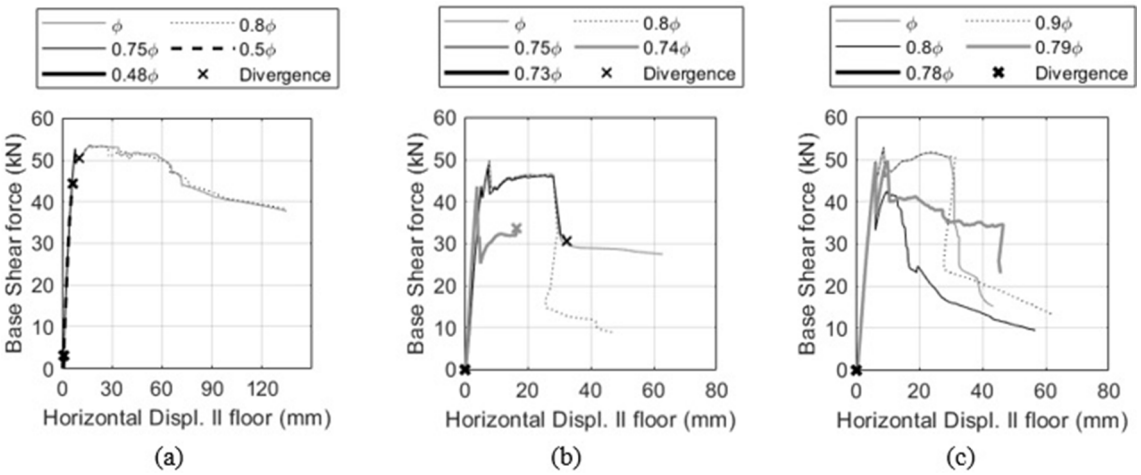

Fig. 18. Capacity curves in terms of Base Shear force vs Horizontal Displacement of the second floor varying the friction angle for (a) EMM-Shell, (b) TSCM-Shell and (c) TSCM-Solid, adopting Coulomb friction interfaces.

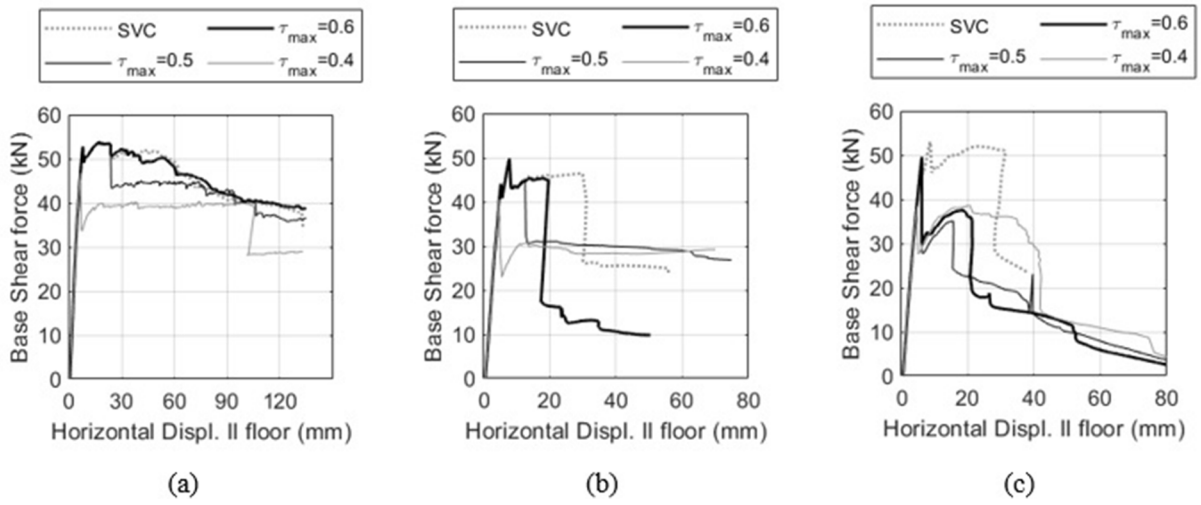

Fig. 19. Capacity curves in terms of Base Shear force vs Horizontal Displacement of the second floor, varying the maximum shear stress for (a) EMM-Shell, (b) TSCM-Shell and (c) TSCM-Solid, adopting Nonlinear Elastic interfaces.

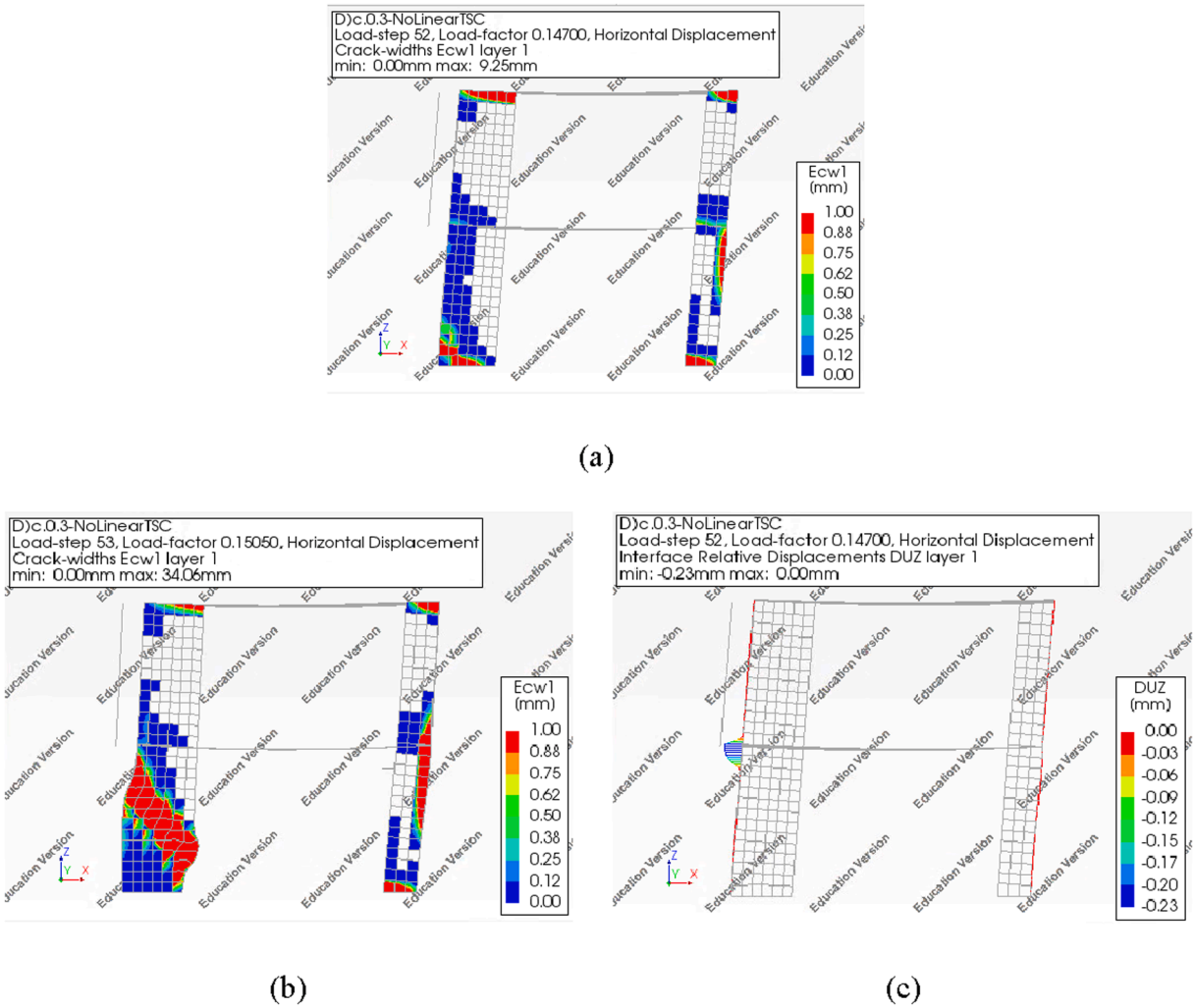

Fig. 20. TSCM-Shell with maximum shear stress equal to 0.6 N/mm^2: (a) and (b) mechanism which causes the decrease of capacity [Output Plot: Crack-widths], (c) sliding of the interface [Output Plot: Interface Relative Displacement].

sensitive to small variations of the friction angle. Besides, similarly to the analyses performed for the U-shaped assemblage, the solution becomes numerically unstable at the onset of the sliding along the interfaces.

Subsequently, the vertical interfaces were modelled via the uncoupled Nonlinear Elastic relations, instead of the coupled non-associated

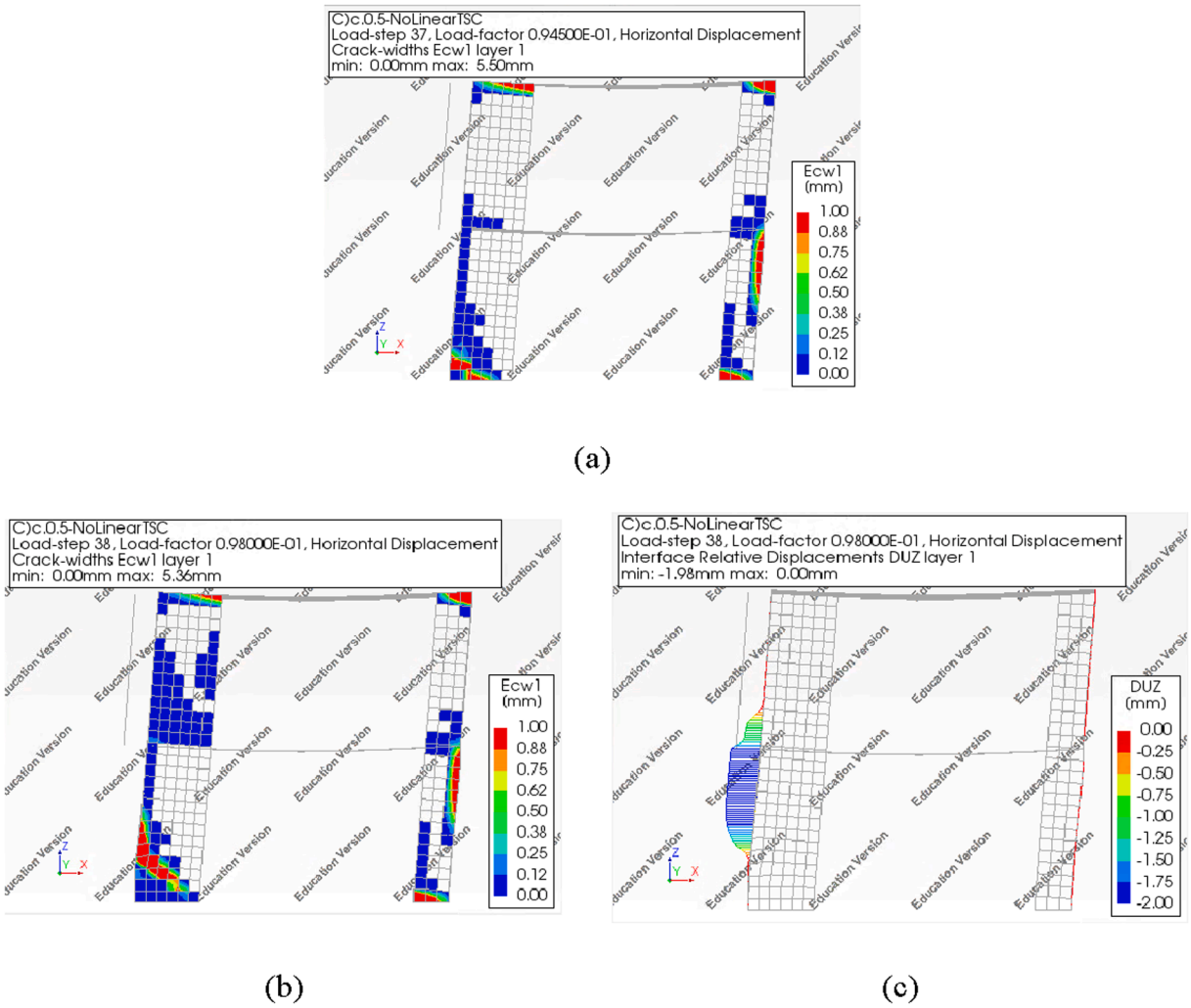

Fig. 21. TSCM-Shell with maximum shear stress equal to 0.5 N/mm^2: (a) and (b) mechanism which causes the decrease of capacity [Output Plot: Crack-widths], (c) sliding of the interface [Output Plot: Interface Relative Displacement].

plasticity-based Coulomb friction model. Also in this case, a sensitivity study was performed by varying the values of the maximum and residual shear stresses of the vertical interfaces.

Fig. 19 shows the comparison of the capacity curves obtained for positive imposed displacements, considering three different values of the maximum shear stress (τ_{max} = 0.4, 0.5, 0.6 N/mm^2), and that obtained by neglecting the nonlinear mechanisms of the vertical joints, i.e. considering strong vertical connections (SVC). Unlike the model with

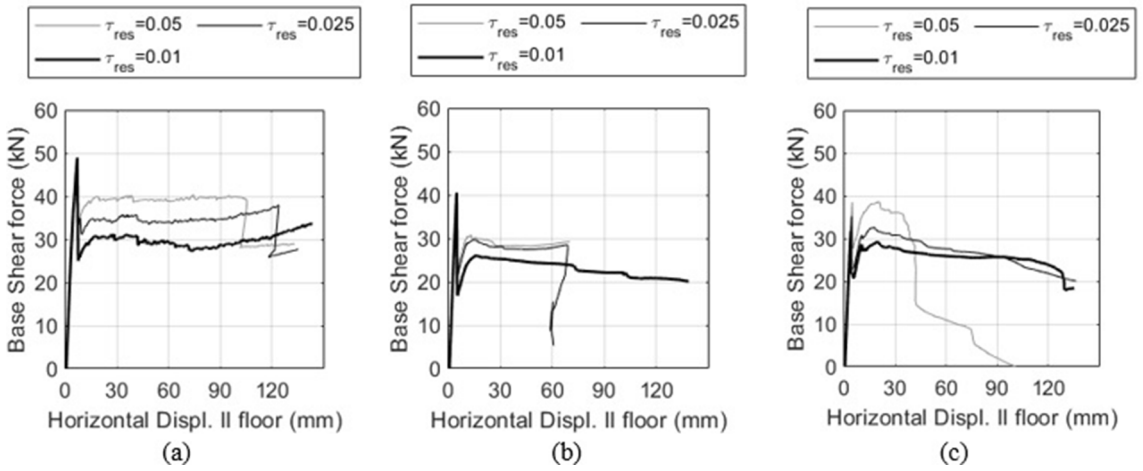

Fig. 22. Capacity curves in terms of Base Shear force vs Horizontal Displacement of the second floor, varying the residual shear stress for (a) EMM-Shell, (b) TSCM-Shell and (c) TSCM-Solid, adopting Nonlinear Elastic interfaces.

Coulomb friction interfaces, more stable numerical results were obtained. In fact, no convergence problems occurred, and the results do not show a significant sensitive to the small variations of the parameters.

Different failure mechanisms occur depending on the strength assigned to the vertical interfaces. In the following, this is discussed with reference to the case of TSCM-Shell. When the vertical joint at the corner is strong, such as for the SVC case, the sudden drop of the force solely depends on the development of a diagonal crack in the wide pier. Conversely, when the value of the maximum shear stress was reduced, a mixed failure mode that combines the diagonal crack with the sliding along the vertical joint was observed, as shown in Fig. 20 and Fig. 21. The two figures also show that a lower value of the maximum shear strength of the connection on the one hand anticipates the global failure of the structure, on the other hand reduces the width of the crack, which also propagates more along the vertical joint. This allows for a higher residual capacity of the structure that is still able to withstand larger deformations.

The effect of the variation of the residual shear stress is limited since this only affects the post-peak capacity of the structure, as illustrated in Fig. 22. Lower values of the residual shear stress reduce the residual capacity but increase its ductility, since the occurrence of further brittle failures is prevented, such as the diagonal cracking of the wide pier.

5. Conclusions

Continuous vertical joints represent a critical detail in Dutch terraced houses built after the 1980s, since their failure may affect the global seismic performance of the building. In numerical models, interface elements are often used to simulate the nonlinear behaviour of the connection. The use of different constitutive laws for interface elements is investigated in this work, first at component level, for U-shaped pier-wall configurations, and then at the full-scale structural level for a two-storey masonry house. The normal-shear coupled plasticity-based Coulomb Friction model is typically adopted, as this describes properly the mechanical behaviour of the joint. However, the analyses performed in this study show that this constitutive law implemented in a FEM framework may not be sufficiently robust to simulate the brittle failure of the continuous vertical joint. In fact, the sudden propagation of the crack leads often to the divergence of the analysis. To overcome these limitations, a simpler Nonlinear Elastic constitutive law with direct, uncoupled uniaxial traction – relative displacement relations for the shear and normal directions is proposed as an alternative. The stiffness matrix of this constitutive law is characterized by decoupled terms in the normal and tangential direction, which is demonstrated to improve the robustness of the model and facilitate the convergence of the analysis. However, the Nonlinear Elastic model has strong limitations too. It requires the accurate calibration of the parameters (maximum and residual shear stress) which define the uniaxial shear diagram. Additionally, this model can only simulate the average behaviour of the elements along the connection, as the shear capacity should be a function of the normal stress, which varies along the height of the connection. In conclusion, the results of this work suggest that further investigations are required to develop and implement a specific constitutive law for interface elements, capable to be more robust during the brittle shear failure governed by Coulomb-friction behaviour.

Additionally, the sensitivity study shows that the capacity of the buildings depends on the strength of the continuous vertical joint. In particular, the base shear force depends on the shear strength of the connection, whereas the residual shear stress determines the post-peak capacity. It is remarkable that the occurrence of the shear failure along the vertical joint does not always have a negative impact on the building performance, since it may prevent - as a fuse action - the further development of brittle failure mechanisms (such as the diagonal cracking of the piers), leading to a partly counter-intuitive increase of the ductility of the structure.

Finally, the outcomes of analyses performed with three different numerical models, including the use of two different constitutive laws for masonry, as well as different elements (shell vs solid), have been compared with the results of a test on a full-scale two-storey building. The results show that the selection of the constitutive law for masonry (in this study the Engineering Masonry Model or Total Strain Crack Model) strongly influences the activation of different failure mechanisms and, hence, the response of the structure. Conversely, the use of solid or shell elements does not have large influence on the outcomes of the analyses.

Declaration of Competing Interest

The authors declare that they have no known competing financial interests or personal relationships that could have appeared to influence the work reported in this paper.

Acknowledgements

This work has been developed as a jointed research cooperation between Sapienza University of Rome and Delft University of Technology, partly funded by the Sapienza thesis abroad scholarship program, herein gratefully acknowledged.

References

[1] Rots, J.G., Van der Pluijm, R., Vermeltfoort, A.Th. and Janssen, H.J.M. (Eds.) Structural masonry: an experimental-numerical basis for practical design rules. Dutch version CUR report 171, 1994, English version A.A. Balkema, Rotterdam, 152 pp., 1997.

[2] Raijmakers, T. M. J. and Van der Pluijm, R. Stability of the calcium silicate piers. *TNOBouw Report BI-91-0219* (1992).

[3] Fehling, E., Stuerz, J., Emami A. Test results on the behaviour of masonry under static (monotonic and cyclic) in plane lateral loads. Deliverable D7.1a,ESECMaSE Project (2007), http://www.esecmase.org.

[4] Magenes, G., Morandi, P., Penna, A. Test results on the behaviour of masonry under static cyclic in plane lateral loads. Deliverable D7.1c, ESECMaSE Project (2008), http://www.esecmase.org.

[5] Mayer U, Caballero Gonzaléz A. ESECMaSE—shaking table tests at the national technical university in Athens. In 14th international brick and block masonry conference, Sydney. 2008.

[6] Esposito, R., Terwel, K., Ravenshorst, G., Schipper, R., Messali, F., and Rots, J. Cyclic pushover test on an unreinforced masonry structure reseambling a typical Dutch terraced house. In Proceedings of the *16th World Conference on Earthquake Engineering,* Santiago, Chile (2017), pp. 1-12.

[7] Esposito R, Messali F, Ravenshorst GJP, Schipper HR, Rots JG. Seismic assessment of a lab-tested two-storey unreinforced masonry Dutch terraced house. Bull Earthquake Eng 2019;17(8):4601–23.

[8] Mariani, V., Messali, F., Hendriks, M. and Rots, J. Numerical modelling and seismic analysis of Dutch masonry structural components and buildings. In Proceedings of the *16th World Conference on Earthquake Engineering,* Santiago, Chile (2017).

[9] Messali, F., Pari, M., Esposito, R., Rots, J.G., and Den Hertog, D. Blind predictions of a cyclic pushover test on a two-storey masonry assemblage: a comparative study. In Proceedings of the *16th European Conference on Earthquake Engineering*, Thessaloniki, Greece (2018).

[10] Graziotti F, Tomassetti U, Kallioras S, Penna A, Magenes G. Shaking table test on a full scale URM cavity wall building. Bull Earthquake Eng 2017;15(12):5329–64.

[11] Miglietta M, Damiani N, Guerrini G, Graziotti F. Full-scale shake-table tests on two unreinforced masonry cavity-wall buildings: effect of an innovative timber retrofit. Bull Earthquake Eng 2021;19(6):2561–96.

[12] Tomassetti U, Correia AA, Candeias PX, Graziotti F, Campos Costa A. Two-way bending out-of-plane collapse of a full-scale URM building tested on a shake table. Bull Earthquake Eng 2019;17(4):2165–98.

[13] Graziotti F, Tomassetti U, Sharma S, Grottoli L, Magenes G. Experimental response of URM single leaf and cavity walls in out-of-plane two-way bending generated by seismic excitation. Constr Build Mater 2019;195:650–70.

[14] Sharma S, Tomassetti U, Grottoli L, Graziotti F. Two-way bending experimental response of URM walls subjected to combined horizontal and vertical seismic excitation. Eng Struct 2020;219:110537. https://doi.org/10.1016/j.engstruct.2020.110537.

[15] Kallioras, S., Grottoli, L., Graziotti, F. "Quasi-static cyclic tests on U-shaped unreinforced masonry walls made of calcium-silicate bricks and blocks", EUCENTRE Research Report EUC092/2020U, EUCENTRE, Pavia, Italy. Available at www.eucentre.it/nam-project, (2020).

[16] Magenes, G., and Penna, A. Seismic Design and Assessment of Masonry Buildings in Europe: Recent Research and Code Development Issues. In Proceedings of *9th Australasian Masonry Conference,* Queenstown, New Zealand (2011).

[17] Calderini C, Cattari S, Lagomarsino S. In-Plane Strength of Unreinforced Masonry Piers. Earthquake Eng Struct Dyn 2008;38(2):243–67.

[18] Sacco E, Addessi D, Sab K. New trends in mechanics of masonry. Meccanica 2018; 53(7):1565–9.
[19] Lourenço PB. Computations on historic masonry structures. Prog. Struct. Engng Mater. 2002;4(3):301–19.
[20] Lourenço, P.B. *Computational strategies for masonry structures*. PhD Thesis. Delft University of Technology (1996).
[21] Calderini C, Lagomarsino S. Continuum Model for In-Plane Anisotropic Inelastic Behavior of Masonry. J Struct Eng (ASCE) 2008;134(2):209–20.
[22] Addessi D, Marfia S, Sacco E, Toti J. Modeling approaches for masonry structures. Open Civil Eng J 2014;8(1):288–300.
[23] Addessi D, Di Re P, Sacco E. Micromechanical and multiscale computational modeling for stability analysis of masonry elements. Eng Struct 2020;211:110428.
[24] Lotfi HR, Shing PB. Interface model applied to fracture of masonry structures. J Struct Eng 1994;120(1):63–80.
[25] Gambarotta L, Lagomarsino S. Damage Models for the Seismic Responce of brick masonry shear walls. Part 1: the mortar joint model and its applications. Earthquake Eng Struct Dyn 1997;26(4):423–39.
[26] Alfano G, Sacco E. Combining interface damage and friction in a cohesive-zone model. Int J Numer Meth Eng 2006;68(5):542–82.
[27] D'Altri AM, de Miranda S, Castellazzi G, Sarhosis V. A 3D detailed micro-model for the in-plane and out-of-plane numerical analysis of masonry panels. Comput Struct 2018;206:18–30.
[28] Addessi D. A 2D Cosserat finite element based on a damage-plastic model for brittle materials. Comput Struct 2014;135:20–31.
[29] Gatta C, Addessi D, Vestroni F. Static and dynamic nonlinear response of masonry walls. Int J Solids Struct 2018;155:291–303.
[30] Lotfi HR, Shing PB. An appraisal of smeared crack models for masonry shear wall analysis. Comput Struct 1991;41(3):413–25.
[31] Lourénço PB, De Borst R, Rots JG. A plane stress softening plasticity model for orthotropic materials. Int J Numer Meth Eng 1997;40(21):4033–57.
[32] Pelà L, Cervera M, Roca P. An orthotropic damage model for the analysis of masonry structures. Constr Build Mater 2013;41:957–67.
[33] Rots JG, Messali F, Esposito R, Jafari S, Mariani V. Computational modelling of masonry with a view to Groningen induced seismicity. Proc. SAHC Conference Structural Analysis of Historical Constructions: Anamnesis, Diagnosis, Therapy, Controls 2016:227–38.
[34] Luciano R, Sacco E. Homogenization technique and damage model for old masonry material. Int J Solids Struct 1997;34(24):3191–208.
[35] Gambarotta L, Lagomarsino S. Damage models for the seismic response of brick masonry shear walls. Part II: the continuum model and its applications. Earthquake Eng Struct Dyn 1997;26(4):441–62.
[36] Milani G, Lourenço PB, Tralli A. Homogenised limit analysis of masonry walls, Part I: Failure surfaces. Comput Struct 2006;84(3-4):166–80.
[37] Addessi D, Gatta C, Sacco E. Multiscale analysis of in-plane masonry walls accounting for degradation and frictional effects. Int J Multiscale Comput Eng 2020;18(2):159–80.
[38] Lagomarsino S, Penna A, Galasco A, Cattari S. TREMURI program: an equivalent frame model for the nonlinear seismic analysis of masonry buildings. Eng Struct 2013;56:1787–99.
[39] Sepe V, Spacone E, Raka E, Camata G. Seismic analysis of masonry buildings: equivalent frame approach with fiber beam elements. In: In CA, Caetano E, Ribeiro P, Müller G, editors. Proceedings of the 9th International Conference on Structural Dynamics; 2014. p. 237–44.
[40] Sangirardi M, Liberatore D, Addessi D. Equivalent Frame Modelling of Masonry Walls Based on Plasticity and Damage. Int J Archit Heritage 2019;13(7):1098–109.
[41] Marques R, Lourenço PB. Possibilities and comparison of structural component models for the seismic assessment of modern unreinforced masonry buildings. Comput Struct 2011;89(21-22):2079–91.
[42] Aşıkoğlu A, Vasconcelos G, Lourenço PB, Pantò B. Pushover analysis of unreinforced irregular masonry buildings: Lessons from different modeling approaches. Eng Struct 2020;218:110830. https://doi.org/10.1016/j.engstruct.2020.110830.
[43] Maio R, Ferreira TM, Estêvão JMC, Pantò B, Caliò I, Vicente R. Seismic performance-based assessment of urban cultural heritage assets through different macroelement approaches. J Build Eng 2020;29:101083. https://doi.org/10.1016/j.jobe.2019.101083.
[44] DIANA FEA 10.2 User's Manual. TNO Building and Construction Research. (2019).
[45] Rots JG. Smeared and discrete representations of localized fracture. In: Bažant ZP, editor. Current Trends in Concrete Fracture Research. Dordrecht: Springer Netherlands; 1991. p. 45–59. https://doi.org/10.1007/978-94-011-3638-9_4.
[46] Schreppers G., Garofano A., Messali F. and Rots, J. *DIANA Validation report for Masonry modelling* (TU Delft Report CM-2016-17, DIANA FEA report 2016-DIANA-R1601). Delft University of Technology, Department of Structural Engineering. 143 pp. 15 Feb 2017.
[47] Jafari S, Esposito R, Rots JG. *From Brick to Element: Investigating the Mechanical Properties of Calcium Silicate Masonry*. RILEM Bookseries 2019;18:596–604.
[48] Ravenshorst G., Esposito R., Schipper R., Messali F., Tsouvalas A., Lourens E-M. and Rots, J. *Structural behaviour of a calcium silicate brick masonry assemblage: quasi-static cyclic pushover and dynamic identification test*. Delft University of Technology, Department of Structural Engineering. Version 5, 21 October 2016 (2016).
[49] Feenstra, Rots, J. G., Arnesen, A., Teigen, J.G., and Hoiseth, K.V. *A 3D constitutive model for concrete based on a co-rotational concept*. Computational Modelling of Concrete Structures, Bad Gastein, Austria; Editors: R. de Borst et al. (1998), pp. 13–22.